Electronic Supplementary Material (ESI) for Chemical Communications.

Tuning the P-C Dative/Covalent Bond Formation in R_3P- C_{60} Complexes by Changing the R Group

Rabindranath Lo,[†a] Debashree Manna[†a] and Pavel Hobza[*a,b]

[a.] *Institute of Organic Chemistry and Biochemistry, Czech Academy of Sciences, v.v.i., Flemingovo nám. 2, 16610 Prague 6, Czech Republic.*
[b.] *CATRIN, Palacký University, Šlechtitelů 27, 78371 Olomouc, Czech Republic*
† Both authors contributed equally to this work and can be considered as the first author.
Email: pavel.hobza@uochb.cas.cz

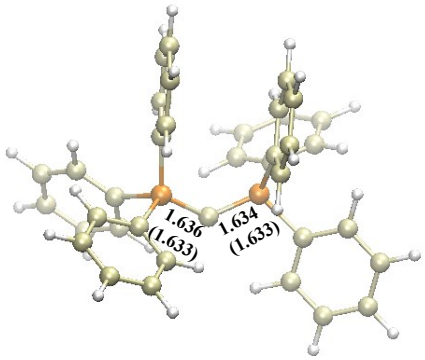

Fig. S1 The optimized structure of hexaphenylcarbodiphosphorane. The bond lengths are in Å. The experimental bond lengths are given in parenthesis and taken from *J. Chem. Soc. Dalton Trans.* **1972**, *5*, 617–622.

Table S1 Total and fragment deformation energies calculated at the PBE0-D3/def2-TZVPP level of theory. The dispersion parts (ΔE_{disp}) of total intrinsic interaction energies (ΔE_{INTR}) are calculated from Grimme's DFT-D3 correction. All values are in kcal/mol.

	$\Delta E_{Def}(C_{60}/BH_3)$	ΔE_{Def}(phosphine)	ΔE_{Def}	ΔE_{disp}
C_{60}...$P(OMe)_3$	23.2	18.7	41.9	-10.8
C_{60}...$P(NMe_2)_3$	24.6	19.5	44.1	-14.1
C_{60}...$P(pyrr)_3$	24.6	16.4	41.0	-15.8
C_{60}...PPh_3	20.7	6.5	27.2	-15.3
H_3B...PPh_3	13.5	1.6	15.1	-3.9

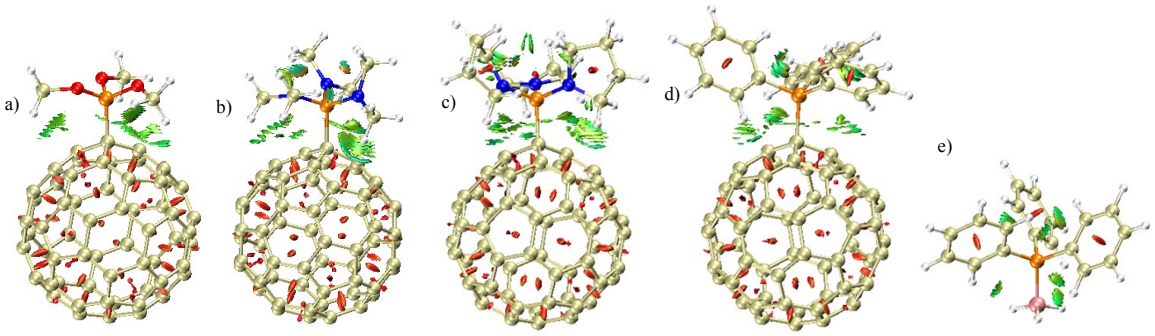

Fig. S2 Three-dimensional NCI surfaces of a) C_{60}...$P(OMe)_3$, b) C_{60}...$P(NMe_2)_3$, c) C_{60}... $P(pyrr)_3$, d) C_{60}... PPh_3, and e) H_3B...PPh_3. The surfaces are coloured according to a blue-green-red scale with a isosurface value of 0.40 a.u. The green indicates attractive interactions and the red marks a strong nonbonded overlap.

Table S2 Calculated interaction energies (ΔE, kcal/mol) and their decomposition into reference and correlation energies from DLPNO-CCSD(T) method.

	ΔE	$\Delta E_{geo\text{-}prep}$	$E_{exch\text{-}rep}$	$E_{elstat} + \Delta E_{no\text{-}disp}$	E_{disp}	$\Delta E_{int}^{C-(T)}$	E_{CT}^{Corr}
C_{60}...$P(OMe)_3$	0.5	41.6	2289.8	-2313.1	-16.7	-1.2	-53.4
C_{60}...$P(NMe_2)_3$	-7.7	44.4	2105.7	-2133.6	-22.4	-1.8	-56.5
C_{60}... $P(pyrr)_3$	-17.5	40.4	2072.0	-2102.4	-25.4	-2.0	-56.4

Table S3 The results of natural bond order (NBO) analysis for various dative bond complexes. The solvent phase results are given in parenthesis.

	NBO Charge Transfer	Wiberg Bond Index	Occupation	P%	X%
C_{60}...$P(OMe)_3$	-1.199	0.806	1.943	38.3	61.7
	(-1.250)	(0.788)	(1.939)	(37.0)	(63.0)[a]
C_{60}...$P(NMe_2)_3$	-1.203	0.787	1.935	38.6	61.4
	(-1.275)	(0.756)	(1.930)	(37.1)	(62.9)[a]
C_{60}... $P(pyrr)_3$	-1.212	0.799	1.937	38.0	62.0
	(-1.276)	(0.774)	(1.932)	(36.7)	(63.3)[a]
C_{60}...PPh_3	-1.049	0.813	1.931	42.9	57.1
	(-1.127)	(0.809)	(1.930)	(41.3)	(58.8)[a]
$(PPh_3)_2C$		1.333	1.971	41.2	58.8[a]
H_3B…PPh_3	-0.688	0.982	1.960	60.4	39.6
	(-0.740)	(0.978)	(1.961)	(59.0)	(41.0)[b]

[a] X = C; [b] X = B

Occupation, a number of electrons, residing in the natural orbital; P%, percentage of NBO electron density, polarized towards the P atom; C%, percentage of NBO electron density, polarized towards the C atom.

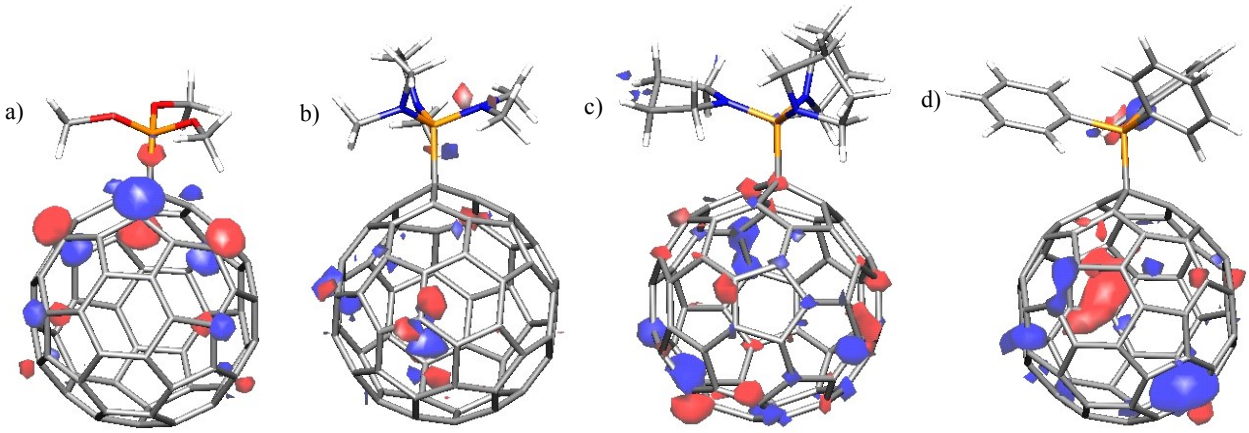

Fig. S3 HOMO frontier molecular orbitals of the optimized dative-bond complexes of C_{60} with different phosphines: a) $P(OMe)_3$, b) $P(NMe_2)_3$, c) $P(pyrr)_3$, and d) PPh_3.

Table S4 The results of atoms in molecules (AIM) analysis for various dative bond complexes. The solvent phase results are given in parenthesis.

	ρ	∇^2_ρ	ε	V	G	|V|/G	H	DI
C_{60}...$P(OMe)_3$	0.189	-0.471	0.0160	-0.2680	0.0751	3.569	-0.1929	0.73
	(0.186)	(-0.424)	(0.0149)	(-0.2765)	(0.0852)	(3.245)	(-0.1912)	
C_{60}...$P(NMe_2)_3$	0.173	-0.436	0.0124	-0.1817	0.0364	4.992	-0.1453	0.73
	(0.167)	(-0.427)	(0.0102)	(-0.1851)	(0.0392)	(4.722)	(-0.1459)	
C_{60}... $P(pyrr)_3$	0.177	-0.440	0.0282	-0.2347	0.0624	3.761	-0.1723	0.71
	(0.171)	(-0.398)	(0.0293)	(-0.2356)	(0.0681)	(3.460)	(-0.1675)	
C_{60}…PPh_3	0.161	-0.347	0.016	-0.1531	0.0332	4.611	-0.1199	0.77
	(0.161)	(-0.370)	(0.015)	(-0.1633)	(0.0355)	(4.600)	(-0.1278)	
H_3B…PPh_3	0.122	-0.036	0.0009	-0.2179	0.1045	2.085	-0.1135	0.48
	(0.124)	(-0.089)	(0.0003)	(-0.2117)	(0.0947)	(2.235)	(-0.1169)	

The following parameters have been calculated for the P-C/P-B bond critical point (3, -1): ρ, the value of electron density (e/bohr^3); ∇^2_ρ the electron density of Laplacian (e/bohr^5); ε, the ellipticity; V, potential energy density; G, kinetic energy density; H, energy density (au/bohr^3); DI, electron delocalization index, the average number of delocalized electrons between quantum atoms C/B and P.

Table S5 Data for the P-C and P-B bonds, obtained from the topological analysis of electron localization function (ELF) of various dative bond complexes. The solvent phase results are given in parenthesis

	N (e)	X|V(X,P) (e)	P|V(X,P) (e)	%P
C_{60}...$P(OMe)_3$	2.146(2.131)	1.335(1.406)[a]	0.811(0.725)[a]	37.8(34.0)
C_{60}...$P(NMe_2)_3$	2.066(2.046)	1.243(1.322)[a]	0.823(0.724)[a]	39.8(35.3)
C_{60}... $P(pyrr)_3$	2.070(2.056)	1.319(1.377)[a]	0.751(0.679)[a]	36.3(33.0)
C_{60}…PPh_3	1.947(1.949)	1.078(1.147)[a]	0.869(0.802)[a]	44.6(41.1)
$(Ph_3P)_2C$	2.629	1.922[a]	0.707[a]	26.9
H_3B…PPh_3	2.026(2.009)	0.231(0.255)[b]	1.795(1.754)[b]	88.6(87.3)

[a] X = C; [b]X = B.

N, the V(X,P) basin population; X|V(X,P), atomic contributions of the X atom to the V(X,P) basin; P|V(X,P), atomic contributions of the P atom to the V(X,P) basin; %P, percentage of electron density for the P atom to the V(X,P) basin population.

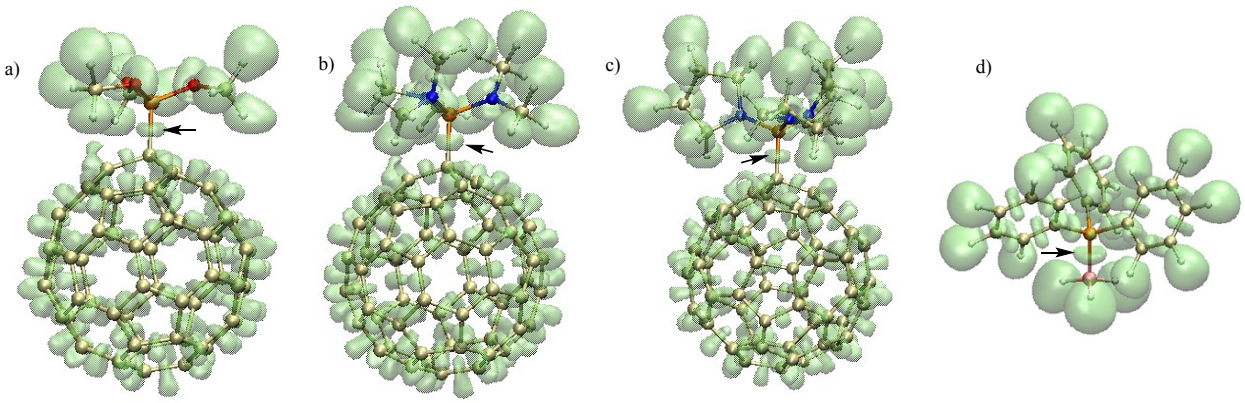

Fig. S4 The isosurface maps of Electron localization function of a) C_{60}...$P(OMe)_3$, b) C_{60}...$P(NMe_2)_3$, c) C_{60}... $P(pyrr)_3$, and d) H_3B…PPh_3 with isovalue of 0.8. The localization domains at the dative bond are marked by arrow.

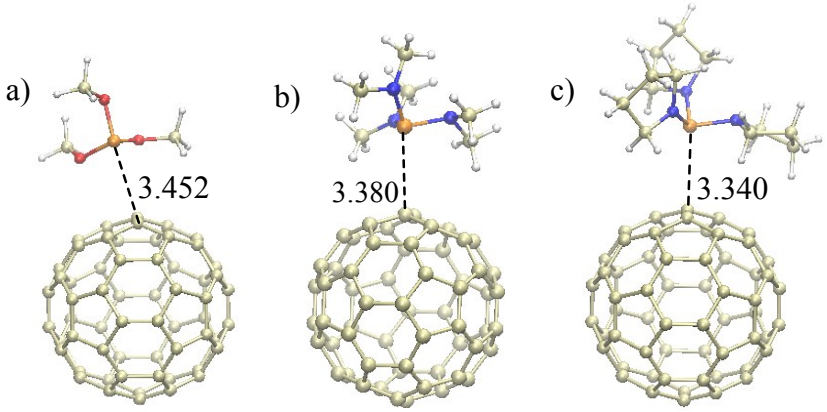

Fig. S5 The optimized vdW complex geometries of a) C_{60}...$P(OMe)_3$, b) C_{60}...$P(NMe_2)_3$, and c) C_{60}... $P(pyrr)_3$. The bond lengths are in Å.

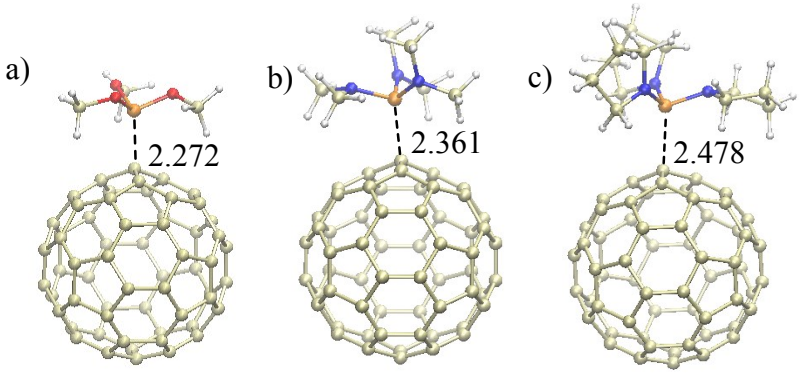

Fig. S6 The optimized transition state geometries of a) C_{60}...$P(OMe)_3$, b) C_{60}...$P(NMe_2)_3$, and c) C_{60}... $P(pyrr)_3$. The bond lengths are in Å.

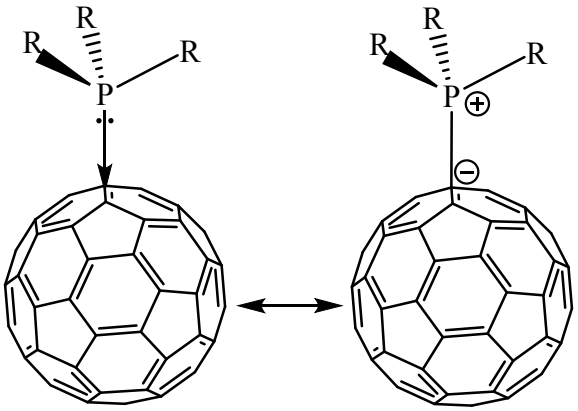

Scheme S1 Lewis formula representations for the phosphine-C_{60} donor-acceptor complexes.

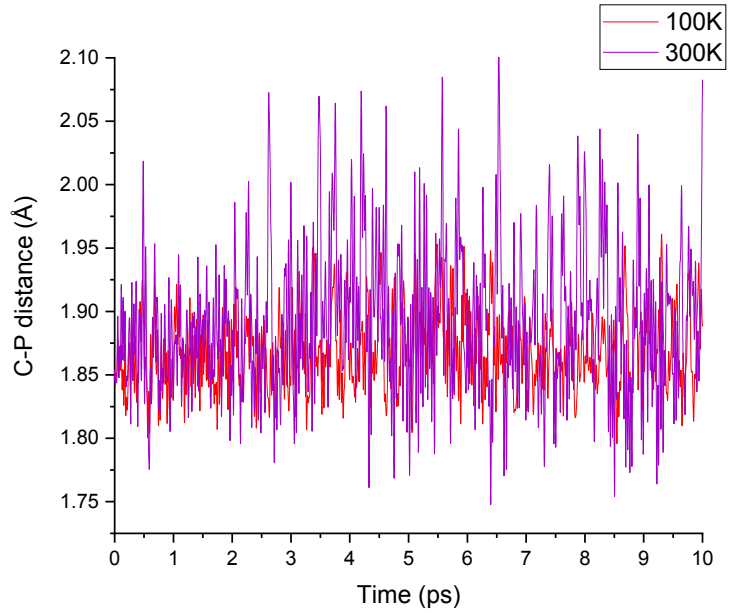

Fig. S7 The variation of the C-P dative bond lengths of the C_{60}...tris(1-pyrrolidinyl)phosphine complex in the trajectory simulated at 100K and 300K.

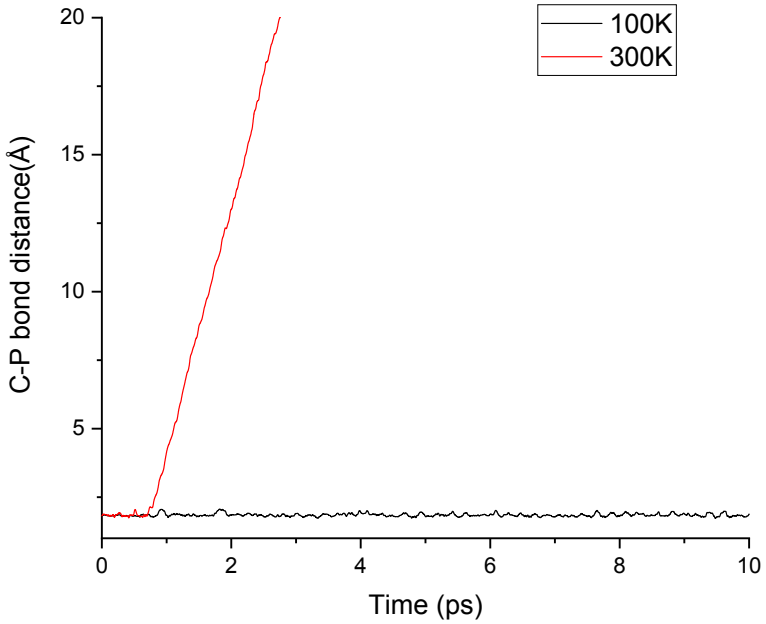

Fig. S8 The variation of the C-P dative bond lengths of the C_{60}...trimethyl phosphite complex in the trajectory simulated at 100K and 300K.

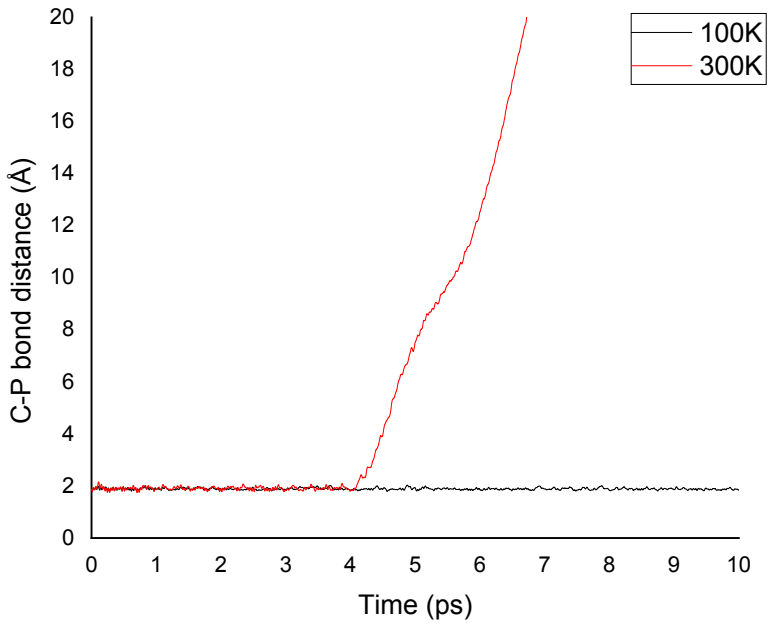

Fig. S9 The variation of the C-P dative bond lengths of the C_{60}...tris(dimethylamino)phosphine complex in the trajectory simulated at 100K and 300K.

Computational details

All the geometries have been fully optimized within C_1 symmetry using the dispersion-corrected-DFT method, employing the PBE0-D3[1,2] functional and def2-TZVPP[3] basis set, whose reliability was confirmed in our previous paper.[4] All interactions are defined in terms of interaction and binding free energies at 298 K at PBE0-D3BJ/def2-TZVPP level. The fully optimized structures of complex and fully optimized isolated monomers have been used to calculate the total interaction energies as

$$\Delta E = E_{complex} - E^{i}_{monomer\,1} - E^{i}_{monomer\,2} \qquad (1)$$

The intrinsic interaction energy (ΔE_{INTR}), defined as a difference between energy of the optimized complex and the sum of the energies of subsystems with geometries taken from the optimized complex geometry.

$$\Delta E_{INTR} = E_{complex} - E_{monomer\,1} - E_{monomer\,2} \qquad (2)$$

The deformation energies (ΔE_{Def}) are defined as energy required to distort the isolated optimized monomers into their complex geometries and it's calculated as a difference of energies of

monomers with the isolated-optimal and complex-optimal geometries. The respective deformation energy is positive.

$$\Delta E_{Def} = \left(E_{monomer\ 1} - E_{\overset{i}{monomer}\ 1}\right) + \left(E_{monomer\ 2} - E_{\overset{i}{monomer}\ 2}\right) \qquad (3)$$

The total interaction energy is thus defined as

$$\Delta E = \Delta E_{INTR} + \Delta E_{Def} \qquad (4)$$

Wiberg Bond indexes (WBI) have been calculated from NBO calculations using the complex geometries optimized at PBE0-D3BJ/def2-TZVPP level.

Domain-based Local Pair Natural Orbital-CCSD(T) (DLPNO-CCSD(T))[5,6] single point calculations were performed for the DFT optimized geometries using def2-SVP basis set. Energy decomposition scheme for the total interaction energy within the DLPNO framework, known as local energy decomposition (LED)[7] was used for detail analysis of interaction energy.

Molecular dynamics trajectories were simulated by ORCA 4.2.1 code[8] and visualized by VMD 1.9.2 visualization software.[9] All the simulations calculated at the PBE0-D3BJ/6-31G* level of theory. The simulation time was performed up to 10 ps. In the simulation, the step size was set to 1 fs, Berendsen thermostat[10] with time constant of 20 fs was employed to control the temperatures. DFT calculations have been performed using Gaussian 16.[11] ORCA 4.2.1[8] was used for the DLPNO-CCSD(T) calculations. The NBO calculations have been performed using NBO 3.1 program[12] as implemented in Gaussian 09. Electron localisation function (ELF) isosurfaces and Non-covalent index (NCI) analyses were carried out using the Multiwfn 3.6 software[13] and plotted using the VMD 1.9.2 visualization software, based on Multiwfn-generated Gaussian cube files. Atoms in molecules (AIM) were calculated using Gaussian files with the Multiwfn 3.6 software. The solvent effects were considered via the COSMO solvation model,[14] with *o*-dichlorobenzene solvent medium.

References

1. C. Adamo and V. Barone, *J. Chem. Phys.*, 1999, **110**, 6158–6170.
2. S. Grimme, J. Antony, S. Ehrlich and H. Krieg, *J. Chem. Phys.*, 2010, **132**, 154104.
3. F. Weigend, *J. Comput. Chem.*, 2008, **29**, 167–175.
4. M. Lamanec, R. Lo, D. Nachtigallová, A. Bakandritsos, E. Mohammadi, M. Dračínský, R. Zbořil, P. Hobza and W. Wang, *Angew. Chemie Int. Ed.*, 2021, **60**, 1942-1950.
5. F. Neese, A. Hansen and D. G. Liakos, *J. Chem. Phys.* 2009, **131**, 064103.
6. F. Neese, A. Hansen, F. Wennmohs and S. Grimme, *Acc. Chem. Res*. 2009, **42**, 641.
7. W. B. Schneider, G. Bistoni, M. Sparta, M. Saitow, C. Riplinger, A. A. Auer and F. Neese, *J. Chem. Theory Comput*. 2016, **12**, 4778.
8. F. Neese, *Wiley Interdiscip. Rev.: Comput. Mol. Sci.*, 2012, **2**, 73–78.
9. W. Humphrey, A. Dalke, K. Schulten, *J. Mol. Graph*. 1996, **14**, 33.
10. H. J. C. Berendsen, J. P. M. Postma, W. F. van Gunsteren, A. DiNola and J. R. Haak, *J. Chem. Phys.* 1984, **81**, 3684.
11. Gaussian 16, Revision A.03, M. J. Frisch, G. W. Trucks, H. B. Schlegel, G. E. Scuseria, M. A. Robb, J. R. Cheeseman, G. Scalmani, V. Barone, G. A. Petersson, et al. Gaussian, Inc., Wallingford CT, 2016.
12. NBO Version 3.1, E. D.Glendening, A. E.Reed, Eds.
13. T. Lu and F. Chen, *J. Comput. Chem*. 2012, **33**, 580.
14. A. Klamt and G. Schüürmann, *J. Chem. Soc. Perkin Trans.2*. 1993, **2**,799–805